Design of Speed Control and Reduction of Torque Ripple Factor in BLdc Motor Using Spider Based Controller

M. Pandi Maharajan and S. Arockia Edwin Xavier

***Abstract*—It is a very difficult process to achieve smooth drivers for the motor operating under variable speed mode. In brushless direct current motor (BLdc) when back electromotive force waveform is of trapezoidal type, the developed torque is constant in ideal conditions. However, practically, torque ripple is present in the output torque because of the physical design of the motor and its parameters. Also, the produced ripples are associated with the control and driver side of the motor. In the previous literature, the drive without a dc-link capacitor is presented but the torque ripple reduction is not effective. Hence in another work, the usage of the small capacitor is recommended and the results are improved. In this work, the quick stabilization with torque ripple reduction is presented using a bio-inspired algorithm-based technique in a BLdc motor drive. A Spider based controller is built to generate the pulsewidth modulation signals applied to the inverter and the control signal applied to the capacitor. The effect of utilizing small dc-link capacitor, on the torque ripple reduction and speed control is investigated. The performance is also compared with the case of large capacitor utilization and without a capacitor case. The proposed control strategy is verified experimentally by implementing with dsPIC30F4011 and the hardware circuit.**

***Index Terms*—Brushless direct current (BLdc) motor, dc-link capacitor, PWM sequence, spider based controller, spider web construction.**

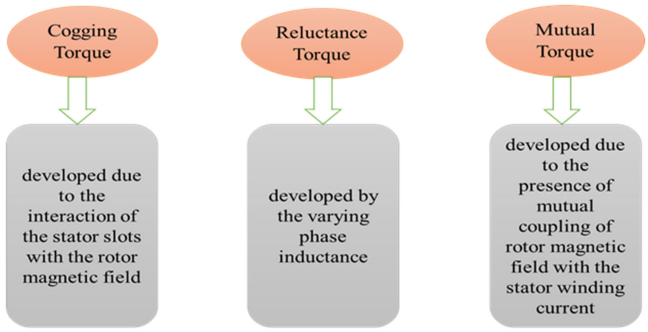

I. Introduction

In recent years, brushless dc (BLdc) motors are widely utilized in various industrial and home applications for example computer peripheral devices, electric vehicles, etc. This motor has numerous advantages like more power density, high power factor, high efficiency, increased reliability, high torque, small size, large life, less noise, less maintenance, and simpler control mechanisms. As the BLdc motor is brushless, the commutation process is performed electronically in this motor. In this kind of commutation, position sensors are employed to obtain rotor position respecting the stator winding. A three-phase BLdc motor

Manuscript received June 20, 2018; revised September 15, 2018; accepted October 26, 2018. Date of publication November 12, 2018; date of current version May 22, 2019. Recommended for publication by Associate Editor A. J. M. Cardoso. *(Corresponding author: M. Pandi Maharajan.)*

M. P. Maharajan is with the NPR College of Engineering and Technology, Dindigul 624401, India (e-mail:

components do not generate greater influence. However, the mutual torque only produces an effective ripple. When the back-EMF and phase current waveform of particular phases are well-coordinated the ripples is considerably reduced. There are two different torque control methods; open loop method and closed-loop control method. In open loop schemes, harmonic injection approach is a widely used technique which reduces mutual and cogging torque ripples by detecting optimal current waveforms. In closed-loop schemes, the feedback is produced to control ripple torque.

Usually, pulsewidth modulated voltage source inverters are employed to operate BLdc motors. But these designs require extra filter components at the input side and output side. The voltage at the dc–link affects the quality of output waveforms and often causes harmonics. A BLdc motor driver involves a diode rectifier, a large dc-link capacitor, and an inverter supplied with rotor position feedback. The dc-link capacitor used in the drive has a large weight and its lifetime varies adversely with the operating temperature. Consequently, the reliability of the drive is affected in the different applications according to the operating temperature. The cost of the capacitor is about 5–12% of the total cost of motor drives and consumes about 4%–15% of total area in the printed circuit board (PCB) of the driver. By designing the drive without employing a dc-link capacitor, the cost and the driver size can be reduced. Still, the torque characteristics are severely affected. Hence a need for a separate control scheme is envisioned to lessen the ripple. In the controllers without dc-link capacitors, the torque ripples present around zero crossings of the power supply. Many control schemes have been presented in the literature for compensating torque ripples.

Biologically inspired design (BID) and biologically inspired algorithm (BIA) apply biological event or an habitant behavior in attaining solutions for the scientific problems. In the industrial sectors, several products have been fabricated by deliberating BID. Biologically inspired algorithms (BIA) are developed by analyzing the activities of the class of insects, animals, and other habitants in order to frame algorithms for manipulating certain tasks. In this paper, the spider web algorithm is applied to generate the PWM sequence for inverter switches and control pulse to the switch controlling the dc-link capacitor. This spider based control algorithm is inspired by the cobweb building activity of spider. The purpose of web building in spider species is to search prey. By adopting the cobweb building activity of spiders, a bio-inspired control algorithm is derived to apply the switching pulses to the switches presenting in the topology. The proposed technique also concerns the issue of torque ripples in the BLdc motor and attempted to lessen the torque ripple causes with small dc-link capacitor. This method also introduces a control method to reduce the ripples without affecting the motor speed. The contribution of this work is the effective reduction of torque with more stabilization in the motor speed which is illustrated in the curves presented in the results section. The operation of the proposed design is compared with the fuzzy-logic based PWM generator and also for various cases based on the utilization of capacitor.

II. Related Works

In many kinds of literature [1]–[4], the authors attempted to reduce the torque ripple in BLdc motors. In [1], the authors demonstrated that the torque ripple is decreased by choosing suitable current harmonics. Hung *et al*. [2] analyzed the torque ripple by analyzing Fourier transforms and the current harmonics are determined. Favre *et al*. [3] computed current harmonics to reduce ripples associated with mutual torque and ripples associated with cogging torque ripple. In [5] and [6], the methods to modify the stator and rotor design were presented to lessen the torque ripples whereas in [7], the windings were modified. In [8]–[15], the controller design is modified to compensate for the torque ripple. In [16], the authors presented technology to lessen the torque ripple caused because of asymmetric motor parameters. In [17], the duty cycle modulation method is presented to reduce ripples produced by nonideal back-EMF. In [18], a feed-forward current control method is presented for a BLdc motor having low inductance. In [19], accelerated torque control method is proposed using the disturbance torque observer. In many works, the torque ripple reduction is attained by amending the controller circuit and algorithms instead of changing the construction of the BLdc motor [20] and [21]. In [22], the work is designed to reduce the torque ripple occurred when the BLdc motor drives do not employ capacitors. In [23], the dual closed loop control strategy of flux linkage and torque is put on to lessen the torque ripple arisen by the nonideal waveform. This work is extended in [24], by using hybrid two and three phase switching mode. In literatures [25]–[31], the braking control techniques are presented. In [25], the ultra-capacitor in conjunction with the bi-directional dc–dc converter is employed to attain braking and energy recovery. In [26]–[29], regenerative braking is employed to reduce ripple. Here, the switching sequence of the switches in the inverter is altered. Zhang *et al*. [30] presented a technique to decrease the current fluctuation produced in braking operation. In [31], the authors implemented various braking modes and braking PWM techniques to small inductance BLdc motor for various speed ranges and hence a smooth brake is obtained. Viswanathan *et al*. [32] presented a technique to reduce torque ripple occurred from the phase current commutation. They employed a dc bus voltage selector circuit, three-level diode clamped multilevel inverter and a modified single-ended primary-inductor converter (SEPIC). Tingna *et al*. [33] presented a torque control strategy. The authors derived the probable combinations of the terminal voltage by changing the switching pulses of the inverter in the normal conduction period and the commutation period. Furthermore, the torque variation rates for various combinations of the terminal voltage are obtained. Then two switching tables are developed using the main vector (MV) and subsidiary vector (SV) based on these derivations. Xinmin *et al*. [34] employed Z-source inverter for torque ripples in BLdc motor. Here, same kind of modulation technique is used in the normal conduction and the commutation periods. The commutation torque ripple is decreased by controlling the active vector and shoot-through vector. The proposed method obtains the terminal of the commutation torque by equating the

clamped terminal voltages with zero reference value. The utilization of Z-source inverter gives the buck-boost competence for BLdc motor and the dc voltage consumption is increased. In [35], Cuk converter is bestowed for torque ripple reduction. The output modes such as the buck–boost and boost modes are changed in commutation and normal conduction period with the help of a proper mode selection block. In the commutation period, the converter works in the boost mode of operation of increase the inverter input voltage and thus the voltage demand of the commutation period is attained. In normal conduction period, the converter works in buck–boost mode and the inverter input voltage is regulated through the pulse amplitude modulation (PAM). Guokai *et al*. [36] presented a configuration by combining a three-level neutral-point-clamped (NPC) inverter and single-ended primary-inductor converters (SEPIC). The authors introduced two-stage converters for torque ripple. The first stage contains two SEPIC converters to achieve the required commutation voltage responding to the motor speed. A dc-link voltage selection circuit is jointly used with the SEPIC module to put on the maximum voltage in the commutation interval. To reduce the torque ripple to more extent, a three-level NPC inverter operates to apply a half reduce the dc-link voltage on the windings.

In [37], a BLdc motor without the dc-link capacitor is presented to reduce the overall cost of the driver. However, when the capacitor is not employed in the drive, the torque ripple is significantly increased in the output. Hence, it is necessary to use a suitable torque ripple compensation technique as provided in the literature above. Still, there is no considerable reduction in torque ripple achieved. Therefore, as the novel technique in [38], low-cost drive employing a small capacitor is presented to remove the drawbacks associated with the capacitor-less drives. In this paper, to develop the control pulses for effectively reducing the torque ripples controller algorithm is developed using cobweb building activity of spider so that the system is stabilized quickly with less torque ripples.

III. Proposed System

In the proposed work, the torque ripple compensation method is presented for a BLdc motor at low cost. The configuration uses a small dc-link capacitor in place of a bulkier capacitor for torque ripple reduction. The capacitance value of the smaller dc-link capacitor connected in this configuration is about 3% of the normally used heavier capacitor.

The mathematical equations of the BLdc motor and the developed torque are given below. To produce the switching sequence, spider web-based controller is employed.

A. BLdc Motor Operation

The pulsating dc is applied to the stator field windings in the BLdc motor. There three pole pairs are considered which are denoted as X, Y, and Z. When dc pulse passes through pair X, the pole X_1 magnetizes as south and the pole X_2 magnetizes as north.

Then the current applied to pole pair X is turned OFF and the pulsated dc passes through pole pair Y and then similarly through pole pair Z. Thus, by giving the pulse to the stator pole pairs sequentially, the magnet will continuously rotate in a clockwise direction.

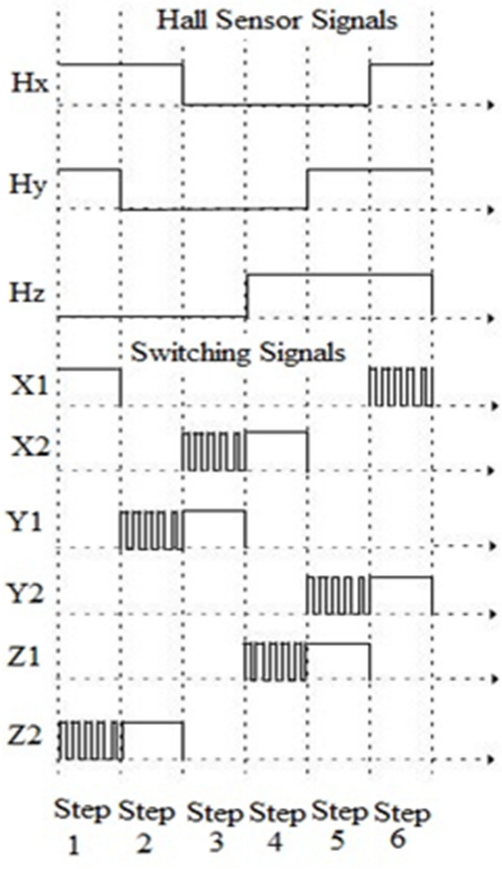

Fig. 2. Hall sensor signals and switching signals [22].

A six-step inverter is employed in the driver side of the motor to work as three-phase supply and the rotating field is created through the electronic commutation of the three pairs of stator coils.

In a three-phase BLdc motor, only two phases are energized at a particular instant, the switches of another phase kept in "OFF" state. Thus, in a particular instant, only two switches of the inverter are kept in "ON" state. In order to control these two switches, the PWM signals are generated from the controller circuit.

The controller circuit is able to operate in two modes namely, torque control or speed control mode [39], [40]. However, in this proposed configuration, the used dc-link capacitor is the small capacitance. Hence, another strategy is proposed for this kind of configuration by controlling only one switch and keeping another switch in "ON" state for the whole interval.

Thus, the obtained switching sequence is given in the table. The switch existing in "ON" state gives a freewheeling path to the inductive current during the "OFF" state of the controlled switch.

The Hall sensor outputs are denoted as H_x, H_y, and H_z. In Fig. 2, the waveforms of Hall sensor output, switching pulses are given along with the rotor position, denoted by ϕ_r.

By taking below assumption, the BLdc motor model is analyzed.

1) BLdc motor is an unsaturated type.
2) The resistances of the stator winding in all the three phases are equal and the inductance (self and mutual) is constant.
3) The semiconductor switches are considered ideal and negligible iron losses are considered.
4) Back-EMF waveforms of all phases are equal.

The dynamic equation models are obtained by considering the equivalent circuit of the BLdc motor and VSI system depicted in Fig. 2

$$V_x = RI_x + (L - M)\frac{di_x}{da} + e_x \tag{1}$$

$$V_y = RI_y + (L - M)\frac{di_y}{da} + e_y \tag{2}$$

$$V_z = RI_z + (L - M)\frac{di_z}{da} + e_z \tag{3}$$

where

V_x, V_y, V_z	Stator phase voltages.
i_x, i_y, i_z	Stator phase current.
e_x, e_y, e_z	Phase back-EMF.
L	Self-inductance.
M	Mutual inductance.
R	Phase resistance.
a	Time instant.

The motion equation is defined as

$$\frac{ds_m}{dt} = \left(\frac{P}{2J}\right)(\tau_e - \tau_L - Fs_r) \tag{4}$$

$$\frac{d\phi}{dt} = s_r \tag{5}$$

τ_e	Electromagnetic torque.
τ_L	Load torque (Nm).
J	moment of inertia (kgm^2).
F	Friction coefficient (Nms/rad).
s_m	Rotor speed in mechanical (rad/s).
s_r	Rotor speed in electrical (rad/s).

Electrical and mechanical speed of the motor are related by

$$Ps = \frac{d\phi_r}{da} \tag{6}$$

where *P* is the number of pole pairs.

B. Modeling of a Trapezoidal Back-EMF Waveform

The trapezoidal back-EMF waveforms are demonstrated with respect to the rotor position by computing the rotor position with respect to the operation speed. The expression of back-EMFs as a function of rotor position (θ_r) is given in the following:

$$e_{xyz} = g_{xyz}(\phi_r) \times E \tag{7}$$

$$E = k_e s_r \tag{8}$$

where (k_e) is back-EMF constant and $g_{xyz}(\phi_r)$ is the function of the rotor position.

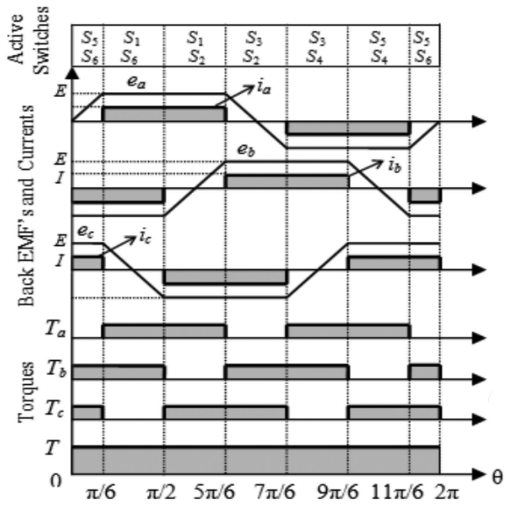

Fig. 3. Trapezoidal back-EMF and phase current waveforms of BLdc motor.

Fig. 3 depicts the waveforms representing trapezoidal back-EMF and phase current. The back-EMF value is a function of rotor position. The trapezoidal shape expression with respect to the rotor position is given in the following:

$$g_x(\phi_r) = \begin{bmatrix} \left(\frac{6}{\pi}\right)\phi_r \ (0 < \phi_r \le 30) \\ 1 \ (30 < \phi_r \le 150) \\ -\left(\frac{6}{\pi}\right)\phi_r + 6 \ (150 < \phi_r \le 210) \\ -1 \ (210 < \phi_r \le 330) \\ \left(\frac{6}{\pi}\right)\phi_r - 12 \ (330 < \phi_r \le 360) \end{bmatrix} \tag{9}$$

$$g_y(\phi_r) = \begin{bmatrix} -1 \ (0 < \phi_r \le 30) \\ \left(\frac{6}{\pi}\right)\phi_r - 4 \ (30 < \phi_r \le 150) \\ 1 \ (150 < \phi_r \le 210) \\ -\left(\frac{6}{\pi}\right)\phi_r + 10 \ (210 < \phi_r \le 330) \\ -1 \ (330 < \phi_r \le 360) \end{bmatrix} \tag{10}$$

$$g_z(\phi_r) = \begin{bmatrix} 1 \ (0 < \phi_r \le 30) \\ -\left(\frac{6}{\pi}\right)\phi_r + 2 \ (30 < \phi_r \le 150) \\ -1 \ (150 < \phi_r \le 210) \\ \left(\frac{6}{\pi}\right)\phi_r - 8 \ (210 < \phi_r \le 330) \\ 1 \ (330 < \phi_r \le 360) \end{bmatrix}. \tag{11}$$

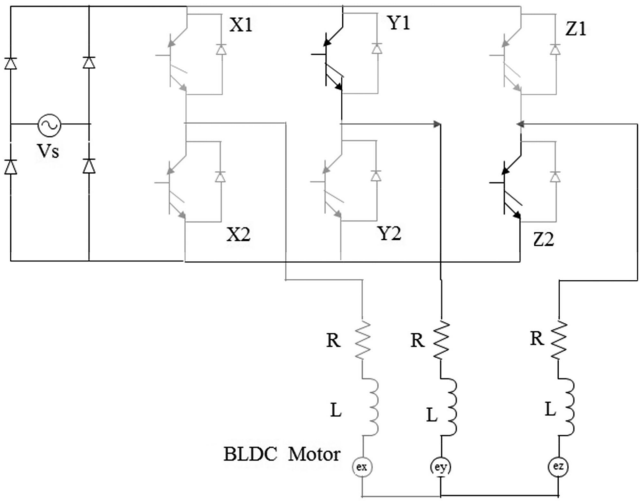

Fig. 4. Step 2 of the switching sequence where Y_1 is ON [22].

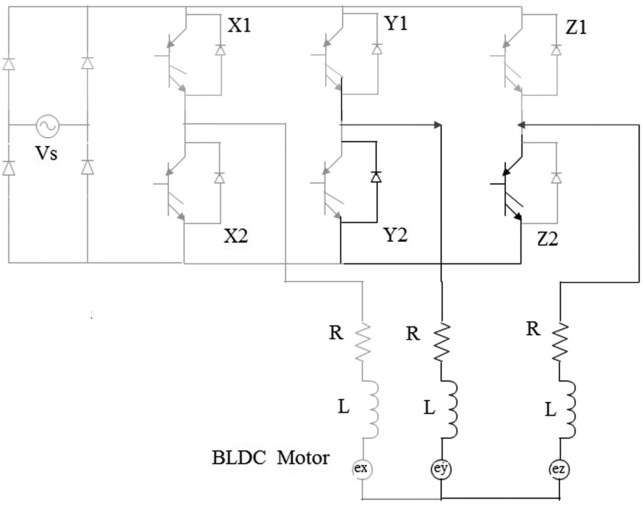

Fig. 5. Step 2 of the switching sequence where Y_1 is OFF [22].

The electromagnetic torque equations for three phases obtained from back-EMF are given in the following:

$$\tau_x = \frac{e_x i_x}{s_r} \tag{12}$$

$$\tau_y = \frac{e_y i_y}{s_r} \tag{13}$$

$$\tau_z = \frac{e_z i_z}{s_r}. \tag{14}$$

The operation of the BLdc drive system corresponding to the second sequence is depicted in Figs. 4 and 5, where switch Y_1 is controlled and Z_2 kept in ON state permanently. The switches connected to phase X are kept in OFF state. Figs. 4 and 5 depict the circuit operation when Y_1 is ON and OFF. From Figs. 4 and 5, it is reflected that the drive operation is similar to that of the buck converter. Thus, the operation of the motor during all the steps of the table can be expressed by the buck converter

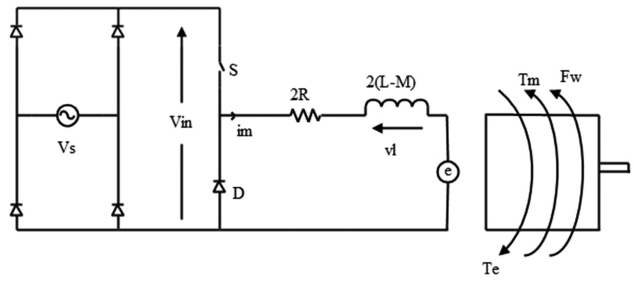

Fig. 6. Buck converter model based BLdc motor driver [22].

model as exposed in Fig. 6. By considering this buck converter model, the motor drive equations are obtained. The notation e(a) in Fig. 6 denotes line-to-line back-EMF, S and D represent the controlled switch and freewheeling diode, respectively.

Based on Fig. 6, the equations representing the BLdc motor drive model are given below

$$v_{\text{in}}\ (a) \ = \ 2i_m\ (a)\, R + 2\,(L - M)\,\frac{di_m\ (a)}{da} + e\,(a) \tag{15}$$

$$0 = \ 2i_m\ (a)\, R + 2\,(L - M)\,\frac{di_m\ (a)}{da} + e\,(a) \tag{16}$$

where v_{in} is the input voltage to the buck converter (V), i_m is the phase current (A), R, L, and M – resistance, inductance, and M is the mutual inductance, respectively.

Assume the value of R is small and so (15) and (16) can be simplified into

$$v_{\text{in}}\ (a) \ = \ 2\,(L - M)\,\frac{di_m\ (a)}{da} + e\,(a) \tag{17}$$

$$0 = 2\,(L - M)\,\frac{di_m\ (a)}{da} + e\,(a)\,. \tag{18}$$

The torque developed by the motor is represented as τ_e and it can be expressed as follows:

$$\tau_e = \frac{e\,(a)\,i_m\ (a)}{s} \tag{19}$$

where ω is the speed of the rotor in rads^{-1}.

The equation of motion of the motor drive is represented as

$$\tau_e - \ \tau_m \ = \ J\frac{ds\,(a)}{dt} + Fs\,(a) \tag{20}$$

where *J* is the combined inertia (kgm^2) of the rotor and load. *F* is the mechanical viscous friction coefficient (Nms).

The relationship between the electrical and mechanical speed of the motor is given by

$$Ps \ = \frac{d\phi_r}{da} \tag{21}$$

where *P* represents the number of pole pairs.

C. Torque Analysis

Usually, the shape of back-EMF waveform is trapezoidal for BLdc motor drives. But, practically, the ideal back-EMF waveform cannot be obtained and it contains some harmonics. In this

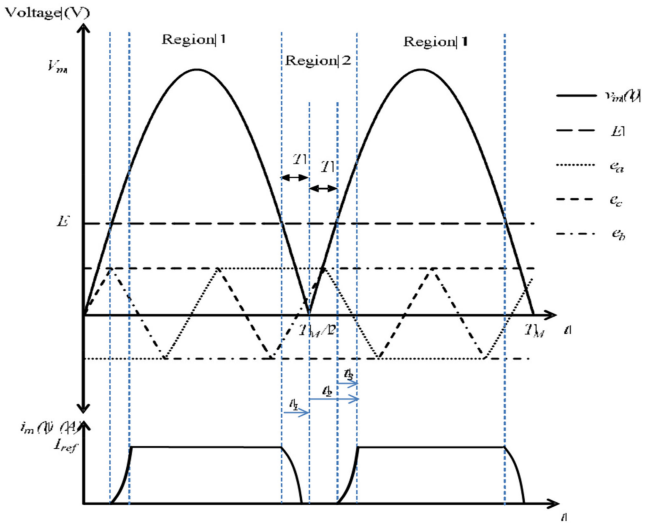

Fig. 7. Regions of the current of the motor drive at steady state [22].

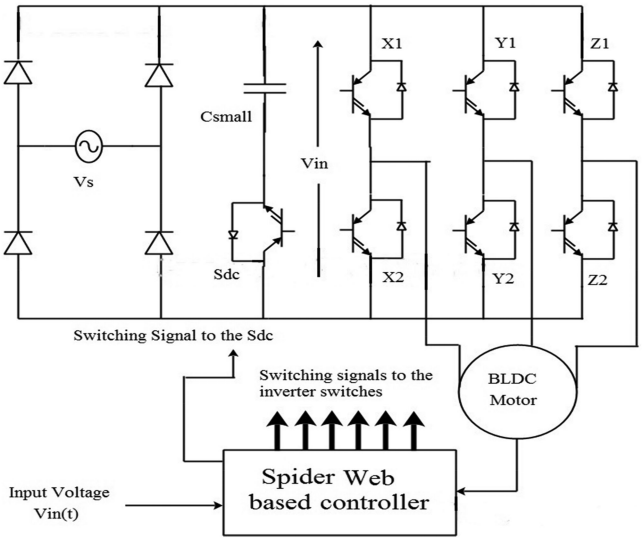

Fig. 8. Proposed technique for torque ripple compensation.

case, the back-EMF produced by the BLdc motor is assumed as the trapezoidal back-EMF. In 120° region of the trapezoidal back-EMF, both the phases of the motor are energized and hence the magnitude of e(a) in this time is E. For simplification in the analysis, the average value of back-EMF is considered as E during 120° period even the back-EMF waveform is not ideally trapezoidal wave.

It is considered that the motor drive is applied with the input voltage v_{in} varying in the range of 0–325 V since the dc-link capacitor is not present. The passing of phase current happens only in one region of rectified supply voltage and when the voltage across the inductance is positive. In Fig. 7, the rectified supply voltage is separated into two regions based on the phase current value. In region 1, the phase current is maintained at I_{ref}, whereas in region 2, it is below I_{ref}.

It is observed from (17) and (18) that since the phase current is non-linear and uncontrollable in region 2, the torque is also uncontrollable in this region. The period of region 2 depends on the back-EMF value and the period is large if the back-EMF is large. The duty cycle of the semiconductor switch is denoted as D(t). It is a time-varying signal that alters for each half cycle of the supply voltage. In region 2, the supply voltage is less than the back-EMF value; hence, the largest possible duty cycle is applied to the switch. Let α be the time interval for the supply voltage $v_{in}(a)$ to reach the value of back-EMF from 0 V and α_i be the time duration of the input supply voltage

$$\alpha = \frac{1}{2\pi f} \sin^{-1}\left(\frac{E}{V_m}\right) \tag{22}$$

where V_m is the peak value (V) of the input supply voltage and f is the frequency (Hz) of the input supply voltage.

In region 2, the current function $i_m(a)$ can be obtained as a piecewise function of time in region 2 and the torque developed by the motor during region 2 can also be obtained as a piecewise function. The variables given in in the following equations are time variables which denote the current function $i_m(a)$

$$\alpha_1 = a - \left[\frac{\alpha_i}{2} - \alpha\right] \tag{23}$$

$$\alpha_2 = a - \left[\frac{\alpha_i}{2}\right] \tag{24}$$

$$\alpha_3 = a - \left[\frac{\alpha_i}{2} + \alpha\right]. \tag{25}$$

The phase current during region 2 is denoted as a piecewise function of time period t_1 using the notation $i_m(\alpha_1)$. Similarly, the voltage across the inductance is denoted as $v_L(\alpha_1)$ where α_1 is in the range of $(\alpha_i/2 - \alpha) \leq a \leq \alpha_i/2$. From Fig. 6, $v_L(\alpha_1)$ can be obtained as

$$v_L\ (\alpha) = -\frac{E}{\alpha}\alpha_1 \tag{26}$$

$v_L(t)$ can be expressed as

$$v_L\ (\alpha a) = 2\,(L - M)\,\frac{di_m\,(a)}{da}. \tag{27}$$

From (25) and (26), the following equation can be derived:

$$2\,(L - M)\ \frac{di_m\,(\alpha_1)}{d\alpha_1} = -\frac{E}{T}\alpha_1. \tag{28}$$

The general time domain solution for (28) can be expressed as

$$i_m\ (\alpha_1) = -\frac{E\alpha_1^2}{4\,(L - M)\,\alpha} + C. \tag{29}$$

By applying the initial condition, as $i_m = I_{ref}$ at $\alpha_1 = 0$, we obtain

$$C = I_{ref}. \tag{30}$$

From (29) and (30), the complete time domain solution for $i_m(\alpha_1)$ can be given as follows:

$$i_m\ (\alpha_1) = -\frac{E\alpha_1^2}{4\,(L - M)\,\alpha} + I_{ref}. \tag{31}$$

From (31), the necessary condition for $i_m(a)$ to be discontinuous before the zero crossing of $v_{in}(a)$ can be mathematically

expressed as follows:

$$(L-M) < \frac{E\alpha}{4I_{ref}}. \tag{32}$$

The value of $i_m(t)$ at the zero crossing is represented as follows:

$$I'_m = \frac{-E\alpha}{4\,(L-M)} + I_{ref}. \tag{33}$$

From Fig. 6, $v_L(t_2)$ can be represented as follows:

$$v_L\ (\alpha_2) = \frac{E}{\alpha}\,\alpha_2 - E. \tag{34}$$

Using (27), we get

$$2\,(L-M)\ \frac{di_m\,(\alpha_2)}{d\alpha_2} = -\frac{E}{\alpha}\alpha_2 - E. \tag{35}$$

The general time domain solution for (35) can be expressed as

$$i_m\ (\alpha_2) = -\frac{E\alpha_2^2}{4\,(L-M)\,\alpha} - \frac{E\alpha_2}{2\,(L-M)\,\alpha} + C. \tag{36}$$

Applying the initial condition expressed in (33) in (36), we obtain

$$i_m\ (\alpha_2) = -\frac{E\alpha_2^2}{4\,(L-M)\,\alpha} - \frac{E\alpha_2}{2\,(L-M)\,\alpha} - \frac{E\alpha}{4\,(L-M)\,\alpha} + I_{ref} \tag{37}$$

Equation (37) gives $i_m(a)$ after the zero crossing of $v_{in}(a)$. Similarly, the necessary condition for the signal $i_m(a)$ to be continuous during the region 2 can be represented as follows:

$$L - M > \frac{E\alpha}{2I_{ref}}. \tag{38}$$

Thus, if the equivalent line-to-line inductance of the motor is below $E\alpha/I_{ref}$, $i_m(a)$ is discontinuous in region 2. Then, $i_m(a)$ begins to increase after $a = \alpha_M/2 + \alpha$, to reach $I_{ref}(a)$.

Similarly, the signal $i_m(a)$ can be represented as a function of α_3 as follows:

$$i_m\ (\alpha_3) = -\frac{E\alpha_3^2}{4\,(L-M)\,\alpha}. \tag{39}$$

Equations (29), (37), and (42) are taken to acquire the instantaneous torque in region 2, the average torque and the reduction of the average torque when the motor is operated in constant speed without the dc-link capacitor.

D. Torque Ripple Compensation

In the proposed drive, torque ripples and discontinuities are generated in region 2 due to uncontrollable phase current. The cause for uncontrollable phase current is that there is no dc-link capacitor. Those ripples and discontinuities are not fit for certain applications where constant torque is required. As a result, the torque ripple reduction technique using a small capacitor dc link is proposed in this work. The capacitor is controlled by the new control algorithm derived from the spider web building method.

1) Capacitance Calculation: In region 1 in Fig. 7, the capacitor C_{small} is charged via antiparallel freewheeling diode of switch A_{DC}. Since there is no natural discharging track for the C_{small}, the discharge can be manipulated by the switching pulse given to A_{DC}. The energy stored in C_{small} must be enough to retain $i_m(a)$ at I_{ref} in region 2 for torque ripple reduction. The controller constructed to obtain that switching pulse given to S_{DC} is got based on E and $v_{in}(a)$. Line-to-line back-EMF, E is computed from the speed of the motor. As C_{small} gives energy to the motor during region 2 only (i.e. when $E > v_{in}(a)$), the size of C_{small} is less compared with a dc-link capacitor presented in a conventional BLdc motor drive. The C_{small} value required to regulate the dc-link voltage in region 2 is given by the following:

$$C_{\text{small}}\ \frac{dV_{\text{in}}\,(a)}{dt} = I_{\text{avg}} \tag{40}$$

where I_{avg} is the average current taken from the dc link to keep $i_m(a)$ at I_{ref}. Obtaining a systematic solution for I_{avg} is a complex process. Since the duty cycle of the switch is time-varying and the current taken from the dc link is of the discrete wave. I_{avg} can be calculated from the simulation model. If I_{avg} is delivered by the dc link during regions 1 and 2, torque ripples can be reduced. From (40), the smallest value of C_{small} can be obtained as in the following to draw I_{avg} from the dc link

$$C_{\text{small}} = \frac{2TI_{\text{avg}}}{V_{\text{in}} - E}. \tag{41}$$

By utilization of the small torque ripple compensation capacitance, scales of the capacitor charging currents are low. Therefore, transient problems in the proposed compensation technique are low. In the proposed topology, an additional control switch is required to control the pulse given to the dc-link capacitor. Hence, the control algorithm must be able to produce the switching signals to the inverter switch as well as to the switch controlling the dc-link capacitor. We introduce a spider-based controller to regulate the switches of the inverter and capacitor switch to obtain more improvement in performance as the added advantage.

E. Spider Based Controller Algorithm

In order to generate the switching sequence given in the table, the control circuit is designed by taking the speed and rotor position as input. The Hall sensor output, which denotes the position of the rotor, is applied to the control circuit. In the control circuit, the back-EMF equation is represented as a function of the rotor position using (7). The back-EMF (E) is compared with the input voltage and the difference is applied to the controller. The controller sends the switching pulse to the switch A_{DC} in relation to the difference. Thus, the dc-link capacitor will either charge or discharge depending on the switching position of the S_{DC} switch, to reduce the torque ripple. When the back-EMF (E) is less than the input voltage ($v_{in}(a)$), the phase current $i_m(a)$ reaches region 2, where it is uncontrollable

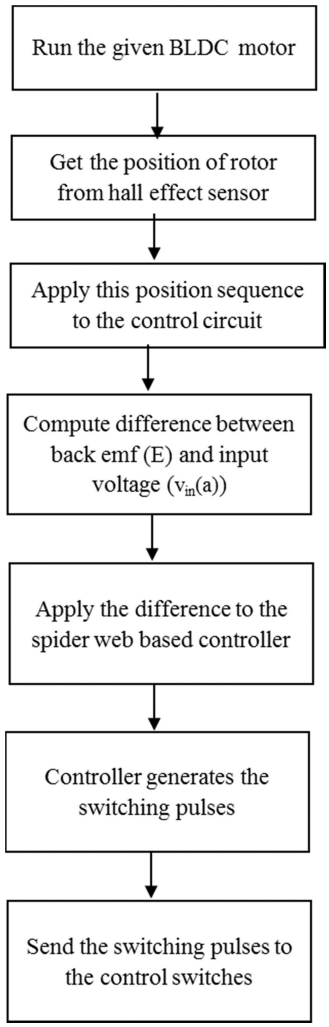

Fig. 9. Flow of the proposed work.

and similarly the torque also becomes uncontrollable. To reduce this torque ripple, the dc-link capacitor must discharge the energy to keep i_m(a) at I_{ref}. To meet out this requirement the capacitor must be charged sufficiently in the charging phase, to supply the sufficient energy in its discharging phase. The discharge time depends on the value of i_m (a) in α_1, α_2, and α_3. Accordingly, the duty cycle of the switch S_D must be varied. Similarly, the PWM patterns to the inverter switches are generated based on the rotor position information. The controller in the proposed work functions based on the spider web building algorithm. The flow of the proposed work is illustrated in Fig. 9.

In the spider based controller, the algorithm gets input and feedback output from the motor to generate the output signal which is switching sequence similar to a web building activity of a spider. In the spider web building process, initially, it produces a silky thread from its mouth. Similar to that the controller gets input signals such as input voltage v_{in} (a), Hall sensor output. After creating silk, the spider thrust it in air to stick at a certain place. The place where it sticks is based

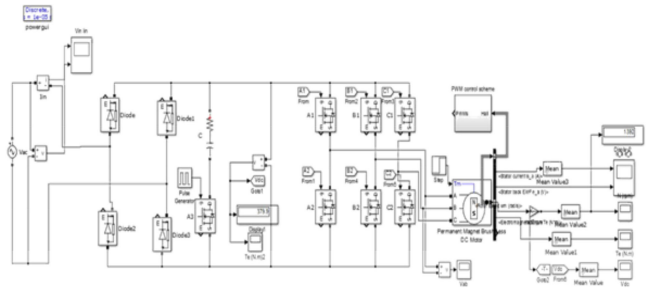

Fig. 10. Simulation diagram.

on the parameters such as the strength of the silk and distance from the spider [41]. As such, this controller work in two modes, in the first mode the spider moves to the input voltage value. Then the spider moves to the Hall sensor output in the second mode. The two modes of operation are explained below.

Mode 1: In this mode, the spider initially has the voltage waveform (thread), it reads the value of the voltage at every instant (searches for the place to fix silk), and then it moves to the zero crossing of the waveform, which is the suitable place where it fixes the silk. From there it moves to another location which is the duty ratio of the switch S_D and fixes silk. Then it moves back to the previous location by eating the previous thread. This operation implies the ON and OFF process of the switch A_{DC}. The duty ratio is obtained as follows:

$$D_{spider} = \frac{\alpha_{on}}{\alpha_{on} + \alpha_{off}}. \tag{42}$$

Mode 2: In this mode, the spider has the Hall sensor signal. From the location, it moves to the suitable place. The suitable place denotes the suitable switch connected to the positive terminal of the supply. Then it fixes thread which implies the switch ON of the process of the respective switch. From that location, it searches another suitable location to fix thread. This location implies the switch connected to the negative terminal of the supply and it should not belong to the same phase of the switch connected to the positive terminal. After choosing the location, the spider fixes thread. Then it moves back and forth between this new location and its previous location by doing any one of the two different actions; namely 1) eat the fixed thread or 2) add an extra thread. This denotes the ON and OFF operation of the switch. Thus, the switch is controlled by suitably adjusting the duty ratio. The number by which the spider should move back and forth is given by the frequency of the operation. The operation of eating the thread and fixing extra thread is computed by ON and OFF time period. The ON-time period is given in (42).

$$\alpha_{on\,spider} = \frac{1}{2\pi f} \sin^{-1}\left(\frac{E}{V_m}\right).$$

The spider based controller algorithm is given below.

Spider Based Controller Algorithm.

1. Goto mode 1.
2. Initially, the spider has the input voltage signal $v_{in}(a)$ //spider has the thread
3. Reads the value of the voltage at every instant //searches for the place to fix silk
4. Moves to the zero crossing of the waveform using Move ($v_{in}(a)$, 0) // move to the suitable place where it fixes the silk
5. Start to operate the switch A_{DC} using Move (0, A_{DC}) // move to another suitable location
6. Control the switch by altering the duty ratio using swapmove() where the spider moves back to the previous position // eat the thread between two locations or add more thread between locations.
7. end // mode 1
8. Goto mode 2.
9. Spider has a Hall sensor signal.
10. Select a suitable switch connected to the positive terminal of the supply using Move(Hall, SP)
11. Switch ON the respective switch using fixsilk(SP) //Fix thread between the locations
12. Select the switch which does not belong to the same phase and connected to the negative terminal of the supply using Move(SP, SN) // move to another suitable location and fix thread
13. while (i <= 1/ total period)
14. Moves back to the previous location (SP) using swapmove().
15. Turn ON the switch using eatthread (SP, SN) // eat thread between locations
16. Moves again to the position denoting SN
17. Turn ON the switch using addthread (SP, SN) // add thread between locations
18. Increment i by 1 and goto step 12.
19. end while
20. end //mode 2

IV. Results and Discussion

In order to evaluate the proposed control algorithm, the topology and the algorithm are implemented in MATLAB. The simulation diagram of the proposed scheme is presented in Fig. 10. The hardware prototype for the configuration is designed and the proposed spider based control algorithm is implemented in DSP based controller dsPIC30F4011. The hardware prototype is shown in Fig. 11. The performance of the proposed strategy is also analyzed and compared with the capacitor case, without the capacitor case, and small capacitor case. The parameters set to the BLdc motor in this work are displayed in Table II. The Hall effect sensors are mounted in the motor to give the rotor position to the DSP controller. In the DSP controller, the spider web-based control algorithm to generate the switching signals to the inverter switches and to S_{DC} is uploaded. The utilization

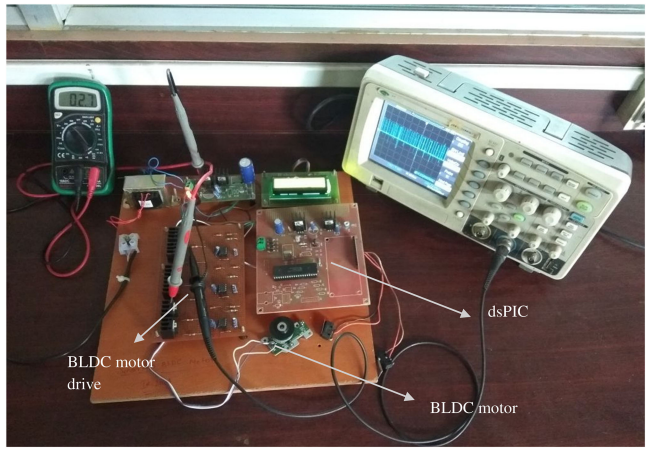

Fig. 11. Hardware prototype.

TABLE I
Switching Algorithm

Step	Hall sensor output			Switch is on state	Controlled switch
	H_a	H_b	H_c		
1	1	0	0	X_1	Z_2
2	1	1	0	Z_2	Y_1
3	0	1	0	Y_1	X_2
4	0	1	1	X_2	Z_1
5	0	0	1	Z_1	Y_2
6	1	0	1	Y_2	X_1

TABLE II
Motor Specifications

Parameter	Notations	Value
Resistance	R	3 Ω
Inductance	L-M	15 mH
Rotor inertia	J	0.0024 kgm^2
Force	F	0.001 Nms
Number of poles	P	3
Back-EMF	E	Trapezoidal
Torque constant	T	0.8 NmA^{-1}
Rated power	P	250 W

of DSP rather than the microcontroller is that the DSPs give faster mathematical operations with integers and floating point operators whereas the microcontroller requires special software operations to work with the floating-point operators. In addition, the implementation cost is reduced with the use of DSP.

Fig. 12(a) and (b) provides a comparison of the phase current (i_m) without a dc-link capacitor nd with a dc-link capacitor. Fig. 12(c) and (d) illustrates the phase current with the small capacitor and with the proposed control algorithm. From Fig. 12, it is detected that the input current becomes discontinuous many times in without capacitor case and small capacitor case.

This is lessened by using the proposed controller and the current is maintained continuously over a long period. In small

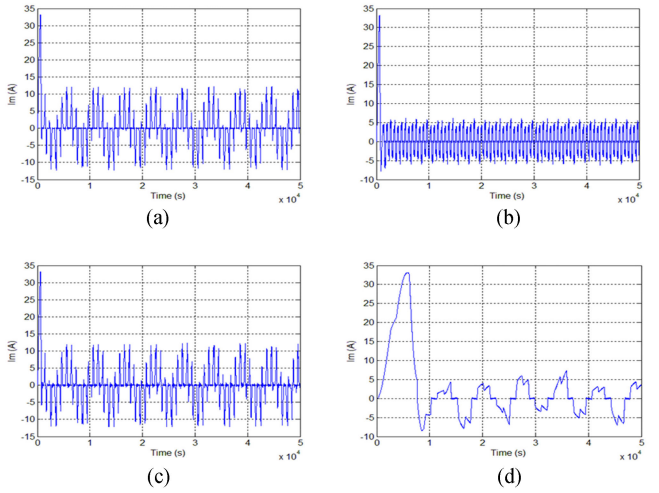

Fig. 12. i_m compensation. (a) Im (A) - without capacitor. (b) Im (A) - with capacitor. (c) Im (A) - with small capacitor. (d) Im (A) - with spider.

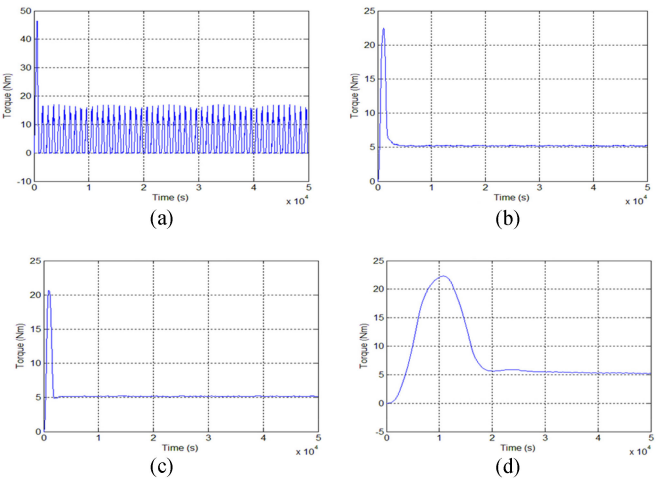

Fig. 13. Torque comparison. (a) Torque (Nm) - without capacitor. (b) Torque (Nm) - with capacitor. (c) Torque (Nm) - with small capacitor. (d) Torque (Nm) - with spider.

capacitor case, the capacitance of 4.7 μF is employed, whereas, in the large capacitor case, 150 μF is used.

Fig. 13(a) and (b) provides a comparison of the torque without a dc-link capacitor and with a dc-link capacitor. Fig. 13(c) and (d) illustrates the torque with the small capacitor and with the proposed control algorithm. From Fig. 13, it is observed that the torque ripples are more in without capacitor case.

When by using large capacitors and small capacitors the ripples are reduced. The reduction is still more when the proposed controller is used in a small capacitor case.

From Fig. 13, it is observed that the rated speed is not constant when the capacitor is not used and it abruptly increases and attains a constant value in with capacitor case.

With the small capacitor, the speed shows small ripples. These are eliminated by using the proposed controller. The speed reaches to the rated value in a linear manner. The output obtained from the experimental implementation is shown in Figs. 14 and 15.

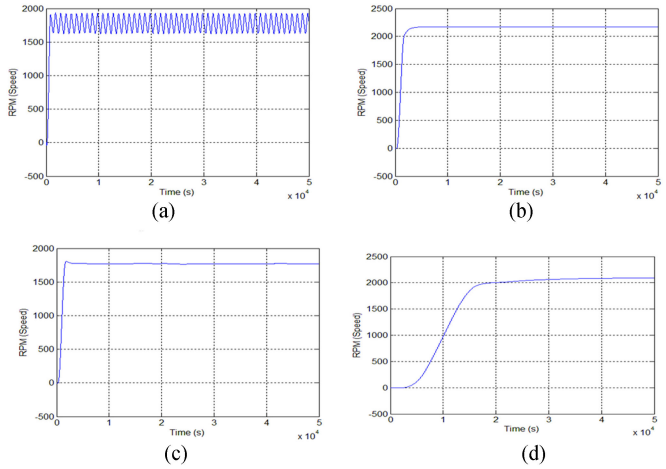

Fig. 14. Speed comparison. (a) RPM (speed) - without capacitor. (b) RPM (speed) - with capacitor. (c) RPM (speed) - with small capacitor. (d) RPM (speed) - with spider.

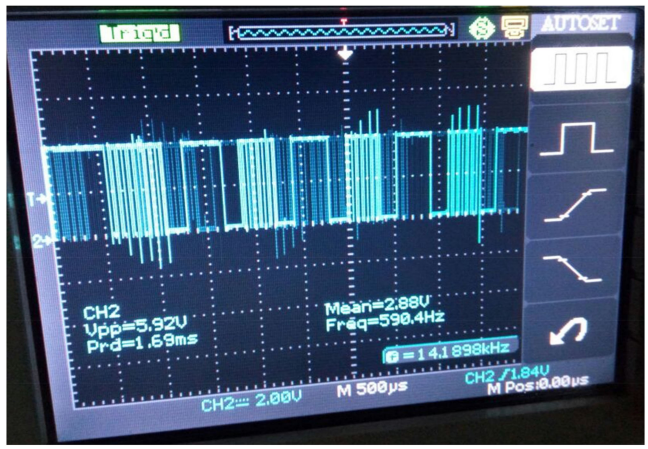

Fig. 15. PWM pulse of switch obtained from spider based controlled algorithm implemented in DSP.

The THD of the proposed work is measured and compared with the THD values obtained for the case with a capacitor, without a capacitor, and with a small dc-link capacitor. It is also observed that the torque ripple is reduced. The compensation torque ripple is not considered since this torque ripple is neglected. Practically, the torque ripple is not reduced completely because of the slower response of the hardware devices.

In this work, the utilization DSP controller is to reduce this effect since the response time of DSP is less than that of the microcontroller. The DSP works faster in computing mathematical operations comparing with the microcontroller. This is the advantage of the proposed implementation. Table III compares the THD presenting in the motor output for different cases as well as the presence of torque ripple.

When a large capacitor based drive is employed, no torque ripple is present, whereas without dc-link capacitor based drive, the torque ripple exist completely, and it is not reduced. In [38], low dc-link capacitor is employed and it is observed that 8% of torque ripples is present. In this work, to quickly reduce the torque, spider web controller is employed and 7% of torque ripples is only present in the outcome.

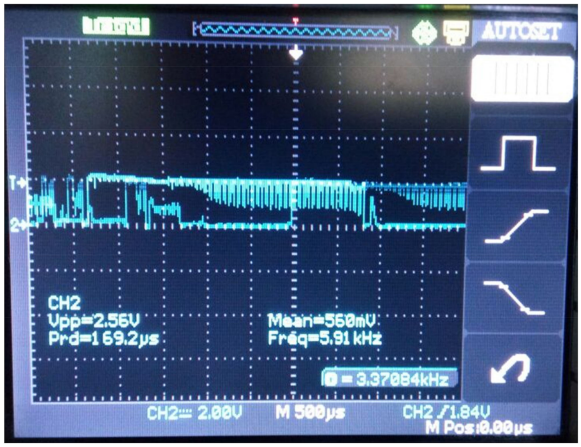

Fig. 16. Current ripple.

TABLE III
COMPARISON OF THD

Case	THD	Torque ripple
With large capacitor	203.4%	0%
Without capacitor	114.3%	100%
With the small capacitor [38]	105.6%	8%
Fuzzy Logic Controller	98.9%	8%
Spider web controller	98.7%	7%

V. CONCLUSION

The method of designing a three-phase BLdc motor drive by using a single-phase voltage source is presented with the intention of employing small dc-link capacitor. In addition, the strategy for reducing torque ripple concern which is generally presenting in BLdc motor is considered in the work. The mathematical equations are developed to determine the capacitor rating and the parameters are set in the simulation to validate the theoretical results. The utilization of a small dc-link capacitor is evaluated by assessing the torque compensation waveform and current compensation waveform with the capacitor-less case and large capacitor case. Besides, the application of spider web building algorithm in generating the necessary switching control pulses are observed by comparing waveforms with the utilization of fuzzy based control algorithm also with the capacitor and without capacitor case. The utilization of spider web-based control algorithm to develop the control pulses make the system to be more stabilized with respect to its speed. Though the scheme has a switch and a small capacitor as additional components, the total price of the drive is reduced. Similarly, the control process used for the switches is simple, extra components are not used. When the large capacitors are used, the motor reliability is reduced since the large capacitors are rated for the small period only. In addition, the simulation results are validated by designing the corresponding hardware using dsPIC30F4011 and the simulation results are validated.

REFERENCES

[1] H. Le-Huy, R. Perret, and R. Feuillet, "Minimization of torque ripple in brushless DC motor drives," *IEEE Trans. Ind. Appl.*, vol. IA-22, no. 4, pp. 748–755, Jul. 1986.
[2] J. Y. Hung, and Z. Ding, "Design of currents to reduce torque ripple in brushless permanent magnet motors," *IEE Proc. B (Electric Power Appl.)*, vol. 140, no. 4, pp. 260–266, 1993.
[3] E. Favre, L. Cardoletti, and M. Jufer, "Permanent-magnet synchronous motors: A comprehensive approach to cogging torque suppression," *IEEE Trans. Ind. Appl.*, vol. 29, no. 6, pp. 1141–1149, Nov./Dec. 1993.
[4] D. C. Hanselman, "Minimum torque ripple, maximum efficiency excitation of brushless permanent magnet motors," *IEEE Trans. Ind. Electron.*, vol. 41, no. 3, pp. 292–300, Jun. 1994.
[5] Z. Q. Zhu, L. J. Wu, and M. L. Mohd Jamil, "Distortion of back-EMF and torque of PM brushless machines due to eccentricity," *IEEE Trans. Magn.* vol. 49, no. 8, pp. 4927–4936, Aug. 2013.
[6] R. Carlson, A. A. Tavares, J. P. Bastos, and M. Lajoie-Mazenc, "Torque ripple attenuation in permanent magnet synchronous motors," in *Proc. IEEE Conf. Record Ind. Appl. Soc. Annu. Meeting*, vol. 1, Oct. 1989, pp. 57–62.
[7] T. R. England, "Unique surface-wound brushless servo with improved torque ripple characteristics," *IEEE Trans. Ind. Appl.*, vol. 24, no. 6, pp. 972–977, Nov./Dec. 1988.
[8] D.-K. Kim, K.-W. Lee, and B.-I. Kwon, "Commutation torque ripple reduction in a position sensorless brushless DC motor drive," *IEEE Trans. Power Electron.*, vol. 21, no. 6, pp. 1762–1768, Nov. 2006.
[9] Y. A. -R. I Mohamed and E. F. El-Saadany, "A current control scheme with an adaptive internal model for robust current regulation and torque ripple minimization in PMSM vector drive," in *Proc. IEEE Int. Elect. Mach. Drives Conf.*, May 2007, vol. 1, pp. 300–305.
[10] S. V. Tewari and B. Indu Rani, "Torque ripple minimization of BLDC motor with un-ideal back-EMF," in *Proc. 2nd Int. Conf. Emerg. Trends Eng. Technol.*, Dec. 2009, pp. 687–690.
[11] H. L. Zhang and L. W. Qu, "A new torque control method for torque ripple minimization of BLDC motors with un-ideal back-EMF," *IEEE Trans. Power Electron.*, vol. 23, no. 2, pp. 950–958, Mar. 2008.
[12] K.-Y. Nam, W.-T. Lee, C.-M. Lee, and J.-P. Hong, "Reducing torque ripple of brushless DC motor by varying input voltage," *IEEE Trans. Magn.*, vol. 42, no. 4, pp. 1307–1310, Apr. 2006.
[13] C.-S. Berendsen, G. Champenois, and A. Bolopion, "Commutation strategies for brushless DC motors: Influence on instant torque," *IEEE Trans. Power Electron.*, vol. 8, no. 2, pp. 231–236, Apr. 1993.
[14] S. B. Ozturk, W. C. Alexander, and H. A. Toliyat, "Direct torque control of four-switch brushless DC motor with non-sinusoidal back-EMF," *IEEE Trans. Power Electron.*, vol. 25, no. 2, pp. 263–271, Feb. 2010.
[15] Y. Zhang, J. Zhu, W. Xu, and Y. Guo, "A simple method to reduce torque ripple in direct torque-controlled permanent-magnet synchronous motor by using vectors with variable amplitude and angle," *IEEE Trans. Ind. Electron.*, vol. 58, no. 7, pp. 2848–2859, Jul. 2011
[16] Y. Xu, N. Parspour, and U. Vollmer, "Torque ripple minimization using online estimation of the stator resistances with consideration of magnetic saturation," *IEEE Trans. Ind. Electron.*, vol. 61, no. 9, pp. 5105–5114, Sep. 2014
[17] J. Fang, H. Li, and B. Han, "Torque ripple reduction in BLDC torque motor with nonideal back-EMF," *IEEE Trans. Power Electron.*, vol. 27, no. 11, pp. 4630–4637, Nov. 2012
[18] J. Fang, X. Zhou, and G. Liu, "Instantaneous torque control of small inductance brushless DC Motor," *IEEE Trans. Power Electron.*, vol. 27, no. 12, pp. 4952–4964, Dec. 2012.
[19] J. Fang, X. Zhou, and G. Liu, "Precise accelerated torque control for small inductance brushless DC motor," *IEEE Trans. Power Electron.*, vol. 28, no. 3, pp. 1400–1412, Mar. 2013.
[20] Y. Ohnuma and J. Itoh, "Space vector modulation for a single phase to three phase converter using an active buffer," in *Proc. Int. Power Electron. Conf.*, 2010, pp. 574–580.
[21] Y. Ohnuma and J. I. Itoh, "Novel control strategy for single-phase to three-phase power converter using an active buffer," in *Proc. 13th Eur. Conf. Power Electron. Appl.*, 2009, pp. 1–10.
[22] H. K. S. Ransara and K. M. Udaya, "A torque ripples compensation technique for a low-cost brushless DC motor drive," *IEEE Trans. Ind. Electron.*, vol. 62, no. 10, pp. 6171–6182, 2015.
[23] Y. Liu, Z. Q. Zhu, and D. Howe, "Direct torque control of brushless DC drives with reduced torque ripple," *IEEE Trans. Ind. Appl.*, vol. 41, no. 2, pp. 599–608, Mar./Apr. 2005.

[24] Y. Liu, Z. Q. Zhu, and D. Howe, "Commutation-torque-ripple minimization in direct-torque-controlled PM brushless DC drives," *IEEE Trans. Ind. Appl.*, vol. 43, no. 4, pp. 1012–1021, Jul./Aug. 2007
[25] J. W. Dixon and M. E. Ortuzar, "Ultracapacitors + dc–dc converters in regenerative braking system," *IEEE Aerosp. Electron. Syst. Mag.*, vol. 17, no. 8, pp. 16–21, Aug. 2002.
[26] M. J. Yang, H. L. Jhou, B. Y. Ma, and K. K. Shyu, "A cost-effective method of electric brake with energy regeneration for electric vehicles," *IEEE Trans. Ind. Electron.*, vol. 56, no. 6, pp. 2203–2212, Jun. 2009
[27] X. Nian, F. Peng, and H. Zhang, "Regenerative braking system of electric vehicle driven by brushless DC motor," *IEEE Trans. Ind. Electron.*, vol. 61, no. 10, pp. 5798–5808, Oct. 2014.
[28] R. C. Becerra, M. Ehsani, and T. M. Jahns, "Four quadrant brushless ECM drive integrated current regulation," in *Proc. Conf. Rec. IEEE-IAS Annu. Meeting*, 1989, pp. 819–828.
[29] C. C. Hua and S. J. Kao, "Design and implementation of a regenerative braking system for electric bicycles based on DSP," in *Proc. 6th IEEE Conf. Ind. Electron., Appl.*, 2011, pp. 703–707.
[30] J. Z. Zhang, S. J. Li, G. Lu, and Q. X. Zhou, "A novel regenerative braking method of BLDCM for wheeled mobile robot," in *Proc. IEEE Int. Conf. Inf., Autom.*, 2010, pp. 676–681.
[31] X. Zhou and J. Fang, "Precise braking torque control for attitude control flywheel with small inductance brushless DC motor," *IEEE Trans. Power Electron.*, vol. 28, no. 11, pp. 5380–5390, Nov. 2013.
[32] V. Viswanathan and J. Seenithangom, "Commutation torque ripple reduction in BLDC motor using modified SEPIC converter and three-level NPC inverter," *IEEE Trans. Power Electron.*, vol. 33, no. 1, pp. 535–546, Jan. 2018.
[33] T. Shi *et al.*, "A torque control strategy for torque ripple reduction of brushless DC motor with nonideal back electromotive force," *IEEE Trans. Ind. Electron.*, vol. 64, no. 6, pp. 4423–4433, Jun. 2017.
[34] X. Li *et al.*, "Commutation torque ripple reduction strategy of Z-source inverter fed brushless DC motor," *IEEE Trans. Power Electron.*, vol. 31, no. 11, pp. 7677–7690, Nov. 2016.
[35] W. Chen *et al.*, "A novel method of reducing commutation torque ripple for brushless DC motor based on cuk converter," *IEEE Trans. Power Electron.*, vol. 32, no. 7, pp. 5497–5508, Jul. 2017.
[36] G. Jiang *et al.*, "Commutation torque ripple suppression strategy for brushless DC motors with commutation time in multiples of PWM period," in *Proc. IEEE Int. Elect. Mach. Drives Conf.*, 2017, pp. 1–6.
[37] H. K. Samitha Ransara and U. K. Madawala, "A low cost brushless DC motor drive," in *Proc. 6th IEEE Conf. Ind. Electron. Appl.*, Jun. 2011, pp. 2723–2728.
[38] H. K. S. Ransara and U. K. Madawala, "A torque ripple compensation technique for a low-cost brushless DC motor drive," *IEEE Trans. Ind. Electron.*, vol. 62, no. 10, pp. 6171–6182, Oct. 2015.
[39] O. Ellabban and H. Abu-Rub, "An overview for the Z-Source Converter in motor drive applications," *Renewable Sustain. Energy Rev.*, vol. 61, pp. 537–555, 2016.
[40] N. A. Qamar and C. J. Hatziadoniu, "Cancellation of selected stator harmonics in BLDC by using an adaptive feedforward controller," *Elect. Power Syst. Res.*, vol. 154, pp. 88–94, 2018.
[41] V. Muneeswaran and M. P. Rajasekaran, "Automatic segmentation of gallbladder using the bio-inspired algorithm based on a spider web construction model," *J. Supercomput.*, pp. 1–26, 2018.

M. Pandi Maharajan received the bachelor's degree from Mohamed Sathak Engineering College, Ramanathapuram, India, in 2007, and the master's degree in power electronics and drives from the Sethu Institute of Technology, Virudhunagar, India, in 2011. He is currently working toward the Ph.D. degree at Thiagarajar College of Engineering, Madurai, India, under Anna University, Chennai, India.

He has more than nine years of teaching experience and has authored/coauthored three papers in reputed journals. His current research interests include special electrical machines, power converter design, DSP-based control of BLDC drives, and automotive applications.

S. Arockia Edwin Xavier received the bachelor's degree in electrical and electronics engineering, the master's degree in power electronics and drives with distinction, and the Ph.D. degree in 1998, 2005, and 2012, respectively, from Anna University, Chennai, India.

He has more than 12 papers published in reputed journals. He is currently working as an Assistant Professor with the Thiagarajar College of Engineering, Madurai, India. His research focuses on applications of power electronics and electrical drives.